

SPATIALLY RESOLVED *SPITZER* SPECTROSCOPY OF THE STARBURST NUCLEUS IN NGC 5253

P. BEIRÃO¹, B. R. BRANDL¹, D. DEVOST², J. D. SMITH³, L. HAO² & J. R. HOUCK²

Draft version October 4, 2018

ABSTRACT

We present new *Spitzer Space Telescope* data on the nearby, low-metallicity starburst galaxy NGC 5253, from the Infrared Array Camera *IRAC* and the Infrared Spectrograph *IRS*¹. The mid-IR luminosity profile of NGC 5253 is clearly dominated by an unresolved cluster near the center, which outshines the rest of the galaxy at longer wavelengths. We find that the [Ne III]/[Ne II] ratio decreases from ~ 8.5 at the center to ~ 2.5 at a distance of ~ 250 pc. The [S IV]/[S III] follows the [Ne III]/[Ne II] ratio remarkably well, being about 4 – 5 times lower at all distances. Our spectra reveal for the first time PAH emission feature at $11.3\mu\text{m}$ and its equivalent width increases significantly with distance from the center. The good anti-correlation between the PAH strength and the product between hardness and luminosity of the UV radiation field suggests photo-destruction of the PAH molecules in the central region. The high-excitation [OIV]25.91 μm line was detected at $0.42 \times 10^{-20} \text{W cm}^{-2}$. Our results demonstrate the importance of spatially resolved mid-IR spectroscopy.

Subject headings: ISM: lines and bands - Galaxies: individual (NGC 5253) - Galaxies: ISM - Galaxies: starburst - Infrared: galaxies

1. INTRODUCTION

NGC 5253 is a nearby, low-metallicity dwarf galaxy with a recent starburst, which is responsible for its infrared luminosity of $L_{IR} \sim 1.8 \times 10^9 L_{\odot}$ (Beck et al. 1996). Distance estimates vary from 3.3 ± 0.3 Mpc (Gibson et al. 2000) to 4.0 ± 0.3 Mpc (Thim et al. 2003); here we will assume 4.0 Mpc, corresponding to $19.4 \text{ pc}''$. With its low metallicity of only about $1/6Z_{\odot}$ (Kobulnicky et al. 1999) NGC 5253 is an excellent target to study starbursts in a low-metallicity environment. The spectral signatures of Wolf-Rayet (WR) stars suggest a very recent starburst (Beck et al. (1996); Schaerer et al. (1997)). Cresci et al. (2005) detected 115 star clusters using optical and near-infrared VLT images at an age range of 3-19 Myr. Turner et al. (1998) found a compact radio source representing a hidden super star cluster (SSC) in one of the earliest phases of SSC formation ever observed. Its ionizing flux corresponds to several thousand O7V star equivalents within the central $2''$ (Crowther et al. 1999; Turner & Beck 2004) and an infrared luminosity of $L_{IR} = 7.8 \times 10^8 L_{\odot}$ (Crowther et al. 1999). Near-infrared observations with Hubble Space Telescope revealed the presence of a double star cluster in the nuclear region, separated by 6 – 8 pc (Alonso-Herrero et al. 2004). There are indications that an interaction with M81 might have provoked the starburst (Kobulnicky et al. 1995).

NGC 5253 has also been studied in the mid-IR with the *Infrared Space Observatory (ISO)* by several authors, e.g., Crowther et al. (1999), Thornley et al. (2000) and Verma et al. (2003). With *Spitzer's* increased sensitivity (Werner et al. 2004) and the smaller slit apertures, the

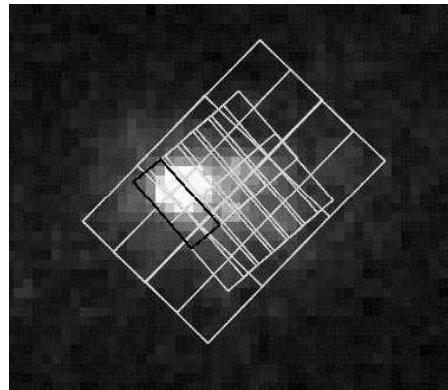


FIG. 1.— Overlay of the SH and LH slits on the *IRAC* $3.6\mu\text{m}$ image of NGC 5253. The image is $1.2' \times 1.0'$. Highlighted is the SH slit at the most central position.

IRS can continue where *ISO* left off. In this letter we report on the spatial variations of the physical conditions in the central region of NGC 5253, based on *IRAC* images and *IRS* (Houck et al. 2004a) spectral maps.

2. OBSERVATIONS AND DATA REDUCTION

The images were obtained on 2005 January 31 using *IRAC* (Fazio et al. 2004) at all four bands ($3.6, 4.8, 5.8, 8.0\mu\text{m}$). The observations consist of 12 slightly dithered pointings of $3 \times 12\text{s}$ exposures each. The data were pipeline processed by the *Spitzer* Science Center. Longward of $5\mu\text{m}$ the *IRAC* images show only one compact cluster and no structure of the host galaxy. To assess what fraction of the total luminosity of the central region is provided by the central cluster we compare the flux within the central 44 pc (2 pixel) to the total flux within a radius of 330 pc for each channel. The results in Table 1 show the increasing dominance of the starburst nucleus in luminosity with wavelength. We subtracted the *IRAC* instrumental PSFs from the nucleus for all four channels, and the residuals suggest that the central cluster remains unresolved in the *IRAC* images, which

¹ Sterrewacht Leiden, P. O. Box 9513, 2300 RA Leiden, The Netherlands

² Astronomy Department, Cornell University, Ithaca, NY 14853-6801

³ Steward Observatory, University of Arizona, Tucson, AZ 85721

¹The *IRS* was a collaborative venture between Cornell University and Ball Aerospace Corporation funded by NASA through the Jet Propulsion Laboratory and the Ames Research Center.

TABLE 1
IRAC FLUX TABLE

λ (μm)	central flux (MJy/sr)	total flux (MJy/sr)	$F_{44\text{pc}}/F_{600\text{pc}}$
3.6	2616 \pm 12	6578 \pm 86	0.39
4.5	5069 \pm 16	7846 \pm 97	0.65
5.8	11640 \pm 29	17187 \pm 261	0.68
8.0	26869 \pm 33	37846 \pm 99	0.71

is consistent with its very compact size (Turner & Beck 2004).

The mid-IR spectra were obtained on 2004 July 14, using high resolution modules ($R \approx 600$) of the *Infrared Spectrograph* (IRS) in spectral mapping mode. In the SH (short-high) mode, the map consists of 12 different pointings, overlapping by half a slit width and about one third slit length, covering an area of $18.0'' \times 23.6''$. In LH (long-high) mode the map consists of only 6 different pointings, covering an area of $22.2'' \times 33.4''$. Fig. 1 shows the SH and LH slit positions overlaid on the IRAC image of the central region. Both maps are slightly off-center. Additional “sky” measurements, 6 arcmin from the nucleus were also taken. The basic processing of the data was performed with version 11.0 of the automated IRS pipeline at the Spitzer Science Center. The background was subtracted using the sky images. The spectra were extracted in “full-slit” mode from pre-flat-fielded files using the IRS data reduction and analysis package SMART, version 5.5 (Higdon et al. 2004). The extracted spectra were flux calibrated with an empirically derived RSRF (relative spectral response function) of α Lac. The spectral overlaps between orders were manually clipped, according to the local S/N. Finally, the SH spectra were scaled up by 16% to match the LH continuum fluxes at $19 \mu\text{m}$. This discrepancy in the fluxes is due to the difference between the SH and LH slit sizes.

3. DISCUSSION

The complete $10 - 38 \mu\text{m}$ SH+LH spectrum at the most central position of our map is shown in Fig. 2. With a smooth continuum with no significant absorption features, and turnover in the slope around $20 \mu\text{m}$, it is dominated by the strong emission lines of [SIV] $10.5 \mu\text{m}$, [NeII] $12.8 \mu\text{m}$, [NeIII] $15.5 \mu\text{m}$, [SIII] $18.7 \mu\text{m}$, [SIII] $33.5 \mu\text{m}$ and [SiII] $34.8 \mu\text{m}$. Also detected are the signature of polycyclic aromatic hydrocarbons (PAH) at $11.3 \mu\text{m}$ and $\text{H}\alpha$ at $12.37 \mu\text{m}$ up to a distance of ~ 120 pc. Fig. 3 shows eight representative SH spectra at decreasing radial distances, calculated from the central cluster to the center of each slit position. The remaining four spectra of our map are redundant and not shown to save space. The most prominent spectral features are labeled. The line fluxes for each radial position are listed in Table 2.

3.1. Gradients in the Radiation Field

With ionization potentials of 21.56 eV and 40.95 eV for Ne and Ne^+ , respectively, the [Ne III]/[Ne II] ratio is a good measure of the hardness of the radiation field, and traces the OB stars. Crowther et al. (1999) measured a relatively low [Ne III]/[Ne II] ratio of 3.5 – 4.0. However, the larger ISO-SWS slit apertures of $14'' \times 20''$

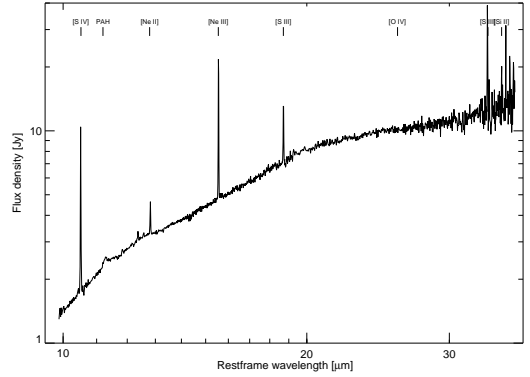


FIG. 2.— Complete IRS SH+LH spectrum of the cluster region of NGC 5253, which correspond to the highlighted slits in Fig. 1. Beyond $35 \mu\text{m}$ the spectrum is dominated by noise and detector artifacts.

and $14'' \times 27''$, centered on the nucleus, may have also picked up significant line flux at lower excitation from the surrounding galactic population. With the smaller IRS slit aperture of $4.7'' \times 11.3''$ we can probe the influence of spatial resolution on the measured spectral diagnostics. The upper plot of Fig. 4 shows the [Ne III]/[Ne II] and [SIV]/[SIII] ratios as functions of the distance to the central cluster. Both ratios decrease by a factor of four over 250 parsecs, indicating a significant softening of the UV radiation field with distance from the cluster core, and trace each other remarkably well, with the Ne ratio being about 4 – 5 times higher at all distances. Our high [Ne III]/[Ne II] ratio at the central cluster is comparable to those observed in nearby H II regions like 30 Doradus and low-metallicity dwarf galaxies like II Zw 40 (Thornley et al. 2000). Rigby et al. (2004) modeled Ne line ratios for star clusters at low metallicity $Z = 0.2 Z_{\odot}$ and showed that a peak ratio of 7.0 is consistent with an upper mass cutoff of $100 M_{\odot}$, at an age of 3 – 5 Myr.

3.2. Dependence of PAH Strength on the Radiation Field

It has often been asked if PAHs in low-metallicity starbursts appear to be weaker because of low abundance or because they get destroyed by the generally harder radiation fields in these environments (e.g., Wu et al. (2005); Engelbracht et al. (2005); O’Halloran et al. (2005); Houck et al. (2004b); Madden (2000)). Our high S/N spectra clearly reveal, for the first time, the presence of the $11.3 \mu\text{m}$ PAH feature in all SH positions on NGC 5253, which shows that PAHs can be present in a low metallicity environment. The center plot of Fig. 4 shows a steady increase of the PAH equivalent width (EW) with distance. We assume constant metallicity throughout the galaxy, as no known dwarf has steep metallicity gradients (Kobulnicky et al. 1999). In Fig. 4 we have investigated the correlation between the measured PAH strength and the “strength” of the UV radiation field, defined by the product of the hardness and the intensity of the radiation field, $[\text{Ne III}]/[\text{Ne II}] \times ([\text{Ne III}] + [\text{Ne II}])$. The bottom plot shows the product between the UV field and the PAH strengths as a function of distance. This product stays almost constant out to a radial distance of 200 pc, mean-

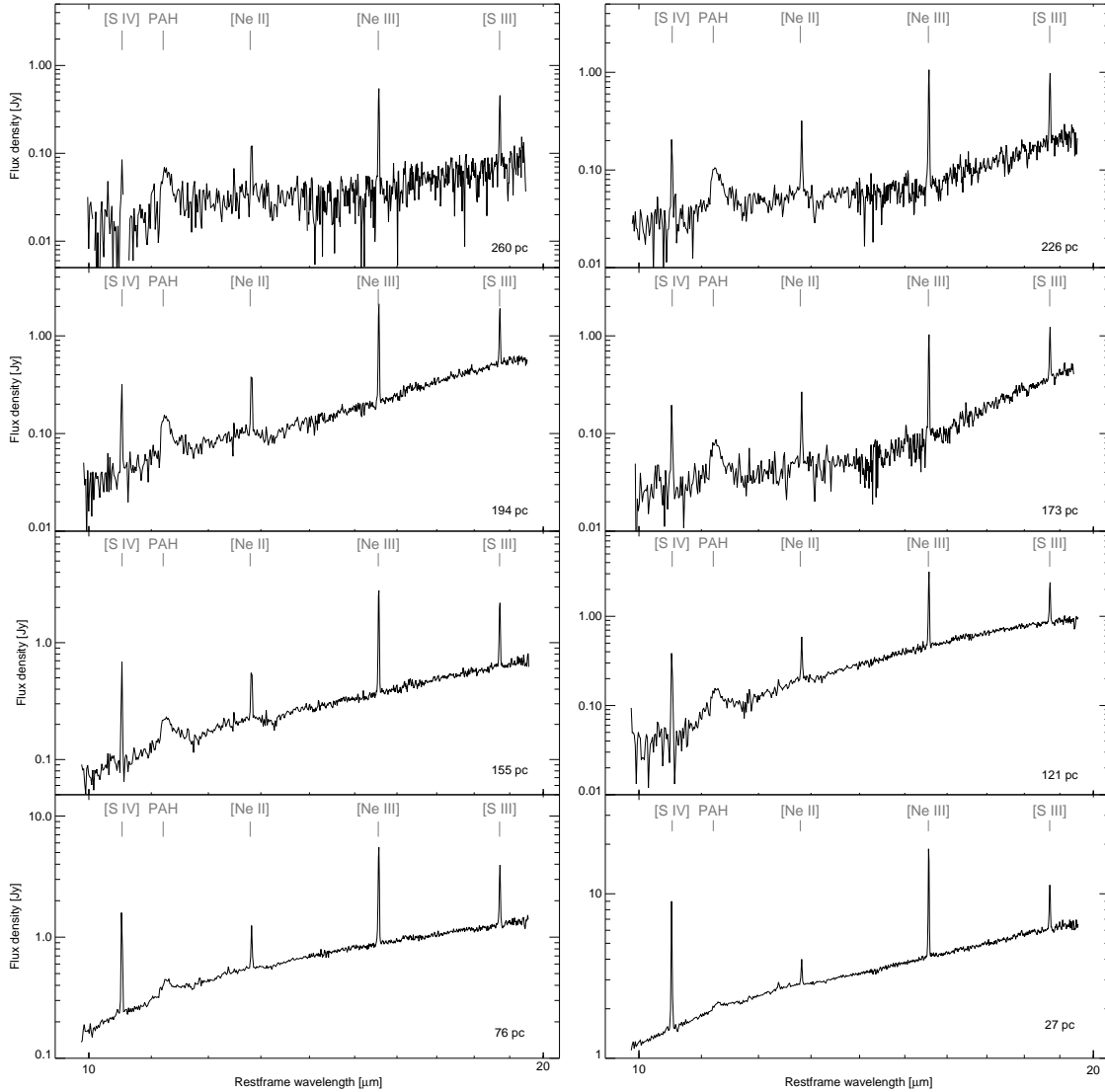


FIG. 3.— IRS SH spectra of NGC 5253 sorted by decreasing distance from the central cluster (from left to right and from top to bottom). The distances are inserted in the lower right of each plot.

ing that the strength of the UV field and the strength of the PAH emission is strongly anti-correlated. The good anti-correlation over such a large distance (encompassing numerous H II regions) suggests that the photo-destruction of PAHs could be the dominant mechanism here. We note that PAH emission models (Li & Draine 2001; Bakes et al. 2001) show that photoionization of hydrogen in PAHs can also cause a decrease in the relative PAH strength above $10\mu\text{m}$. However, we consider this effect unlikely since no ionization effect has been seen in other starburst galaxies (Brandl et al. 2006). For comparison, a low metallicity system like SBS 0335-052, where no PAHs have been detected, has a Ne ratio of 4.9 (Houck et al. 2004b) and some of the low metallicity systems with weak PAHs studied by O’Halloran et al. (2005) have a Ne ratio of $\sim 3 - 4$. As seen in Fig. 4, these ratios correspond to a radial distance inside the PAH destruction zone in NGC 5253.

3.3. [O IV] Line Emission

With an excitation potential of 54.9 eV, the [O IV]25.89 μm line fills the wide energetic gap of mid-IR fine-structure lines between lines that can originate from massive stars and lines that likely require an AGN. It has been attributed to various mechanisms, including very hot stars (Schaerer & Stasinska 1999; Morris et al. 2004) and energetic shocks for low-excitation starbursts (Lutz et al. 1998). Our high S/N spectra reveal a faint [O IV] line at two slit positions outside the central cluster, with fluxes of about $0.42 \times 10^{-20} \text{W cm}^{-2}$ at a S/N of 7.1. This is higher than the limits given by Crowther et al. (1999) ($0.10 \times 10^{-20} \text{W}$), but below the upper limit of Verma et al. (2003) ($0.9 \times 10^{-20} \text{W cm}^{-2}$), and in reasonable agreement with the flux measured by Lutz et al. (1998) ($0.65 \times 10^{-20} \text{W cm}^{-2}$). Using the STARBURST99 code (Leitherer et al. 1999) assuming an instantaneous burst of star formation with a Salpeter

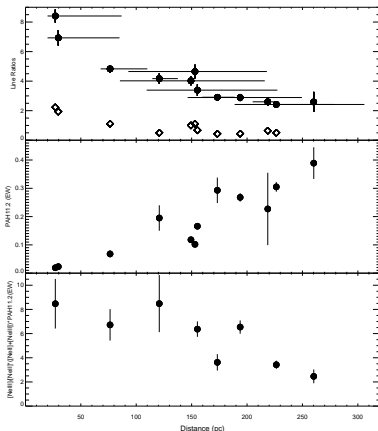


FIG. 4.— *Upper*: Variation of the $[\text{Ne III}]/[\text{Ne II}]$ (full circles) and $[\text{S IV}]/[\text{S III}]$ (diamonds) line ratios with distance to the galactic center. The error bars along the x axis represent the *IRS* slit length, which translates into a range in radial distance; they are the same for $[\text{S IV}]/[\text{S III}]$ ratios. The error bars along the y axis represent flux uncertainties. *Center*: PAH $11.2\mu\text{m}$ equivalent widths (EWs) as a function of distance to the nucleus. The error bars represent EW measurement uncertainties. *Bottom*: Dependence of PAH $11.2\mu\text{m}$ EW $\times ([\text{Ne III}] + [\text{Ne II}]) \times [\text{Ne III}]/[\text{Ne II}]$ with distance. For details see text. The bars indicate systematic errors.

(Salpeter 1955) IMF at 1/5 solar metallicity, the observed OIV emission can be produced by roughly 125 WR stars (WC+WN), consistent with the wide range of O7 V star equivalents (Crowther et al. 1999; Turner & Beck 2004) within the central $1 - 2''$. A detailed discussion is given in Martin-Hernandez et al. (2005). However, as the [OIV] emission is only observed in two LH slit positions off the nucleus, it is not obvious that the [OIV] line is predominantly photo-excited by the central WR stars. Other excitation mechanisms, such as shocks, need to be considered.

This work is based on observations made with the *Spitzer* Space Telescope, which is operated by the Jet Propulsion Laboratory, California Institute of Technology under NASA contract 1407. Support for this work was provided by NASA through Contract Number 1257184 issued by JPL/Caltech.

REFERENCES

- Alonso-Herrero, A., Takagi, T., Baker, A. J., Rieke, G. H., Rieke, M., Imanishi, M., & Scoville, N. 2004, *ApJ*, 612, 222
- Bakes, E. L. O., Tielens, A. G. G. M. & Bauschlicher, Jr., C. W. 2001, *ApJ*, 556, 501
- Beck, S.C., Turner, J. L., Ho, P. T. P., Lacy, J. H., & Kelly, D. M. 1996, *ApJ*, 457, 610
- Brandl, B. R., et al., submitted
- Cresci, G., Vanzì, L., & Sauvage, M. 2005, *A&A*, 433, 447
- Crowther, P.A., Beck, S. C., Willis, A. J., Conti, P. S., Morris, P. W., & Sutherland, R. S. 1999, *MNRAS*, 304, 654
- Engelbracht, C.W., Gordon, K. D., Rieke G. H., Werner, M. W., Dale, D. A., & Latter W. B. 2005, *ApJL*, 628, L29
- Fazio, G. G. et al. 2004, *ApJS*, 154, 10
- Gibson, B. K., et al. 2000, *ApJ*, 529, 723
- Higdon, S. J. U., et al. 2004, *PASP*, 116, 975
- Houck, J. R., et al. 2004, *ApJS*, 154, 211
- Houck, J. R., et al. 2004, *ApJS*, 154, 18
- Kobulnicky, H. A. 1999, in *IAU Symp. 193, Wolf-Rayet Phenomena in Massive Stars and Starburst Galaxies*, ed. K. van der Hucht, G. Koenigsberger, & P. Eenens (San Francisco: ASP), 670
- Kobulnicky, H. A., Kennicutt, R. C., Jr., & Pizagno, J. L. 1999, *ApJ*, 514, 544
- Kobulnicky, H. A., & Skillman, E. D. 1995, *ApJ* 454, L121
- Li, A. & Draine, B. T. 2001, *ApJ*, 554, 778
- Lutz, D., Kunze, D., Spoon, H. W. W., & Thornley, M. D. 1998, *A&A*, 333, L75
- Madden, S. C. 2000, *New A Rev*, 44, 249
- Martin-Hernandez, N. L., Schaerer, D., & Sauvage, M. 2005, *A&A*, 429, 449
- Morris, P.W., Crowther, P. A., & Houck, J. R. 2004, *ApJS*, 154, 413
- O'Halloran, B., Satyapal, S., & Dudlik, R. P. 2005, *ApJ*, accepted
- Rigby, J. R., & Rieke, G. H. 2004, *ApJ*, 606, 237
- Salpeter, E.E. 1955, *ApJ*, 121, 161
- Schaerer, D. & de Koter, A. 1997, *A&A*, 322, 598
- Schaerer, D. & Stasinska, G. 1999, *A&A*, 345, L17
- Summers, L. K., Stevens, I. R., Strickland, D. K., & Heckman, T. M. 2004, *MNRAS*, 351, 1
- Thim, F., Tammann, G. A., Saha, A., Dolphin, A., Sandage, A., Tolstoy, E., & Labhardt, L. 2003, *ApJ*, 590, 256
- Thornley, M. D., Schreiber, N. M. F., Lutz, D., Genzel, R., Spoon, H. W. W., Kunze, D., & Sternberg, A. 2000, *ApJ*, 539, 641
- Turner, J. L., Ho, P. T. P., & Beck, S. C. 1998, *AJ*, 116, 121
- Turner, J. L. & Beck, S. C. 2004, *ApJL*, 602, L85
- Verma, A., Lutz, D., Sturm, E., Sternberg, A., Genzel, R., & Vacca, W. 2003, *A&A*, 403, 829
- Wu, Y., Charmandaris, V., Hao, L., Brandl, B. R., Bernard-Salas, J., Spoon, H. W. W., & Houck, J. R. 2005, in press (*astro-ph/0510856*)
- Werner, M., et al. 2004, *ApJS*, 154, 1

TABLE 2
FINE-STRUCTURE LINES AND RATIOS

distance (pc)	[SIV] ($10^{-20} W cm^{-2}$) $\lambda_{obs} = 10.52 \mu m$ EP=34.8 eV	Hu α ($10^{-20} W cm^{-2}$) $\lambda_{obs} = 12.37 \mu m$	[NeII] ($10^{-20} W cm^{-2}$) $\lambda_{obs} = 12.83 \mu m$ EP=21.6 eV	[NeIII] ($10^{-20} W cm^{-2}$) $\lambda_{obs} = 15.58 \mu m$ EP=41.0 eV	[SIII] ($10^{-20} W cm^{-2}$) $\lambda_{obs} = 18.74 \mu m$ EP=23.3 eV	[NeIII]/[NeII]	[SIV]/[SIII]
27	37.50 \pm 0.21	2.11 \pm 0.53	5.63 \pm 0.14	47.40 \pm 1.21	16.79 \pm 0.58	8.41	2.23
30	33.22 \pm 0.84	1.57 \pm 0.28	5.90 \pm 0.16	40.87 \pm 1.90	17.24 \pm 0.52	6.93	1.93
76	8.80 \pm 0.21	0.43 \pm 0.02	3.51 \pm 0.08	16.94 \pm 0.50	7.91 \pm 0.24	4.83	1.11
121	2.25 \pm 0.32	0.32 \pm 0.10	2.02 \pm 0.09	8.41 \pm 0.31	4.54 \pm 0.16	4.17	0.50
135	7.01 \pm 0.45	...	2.62 \pm 0.17	12.18 \pm 0.33	6.30 \pm 0.18	4.65	1.11
149	6.03 \pm 0.51	...	2.75 \pm 0.13	11.06 \pm 0.25	6.00 \pm 0.12	4.02	1.01
155	3.37 \pm 0.24	...	2.58 \pm 0.23	8.74 \pm 0.14	4.98 \pm 0.09	3.39	0.68
173	1.01 \pm 0.08	...	1.09 \pm 0.02	3.16 \pm 0.11	2.38 \pm 0.08	2.91	0.43
194	1.77 \pm 0.04	...	2.17 \pm 0.14	6.27 \pm 0.09	4.03 \pm 0.09	2.89	0.44
219	0.71 \pm 0.01	...	0.60 \pm 0.04	1.55 \pm 0.06	1.10 \pm 0.07	2.60	0.64
226	1.18 \pm 0.18	...	1.36 \pm 0.08	3.28 \pm 0.11	2.35 \pm 0.09	2.42	0.50
260	0.68 \pm 0.12	1.76 \pm 0.07	1.12 \pm 0.05	2.59	...